Journal of Power Sources 254 (2014) 10–17

Contents lists available at ScienceDirect

Journal of Power Sources

journal homepage: www.elsevier.com/locate/jpowsour

Supercapacitive performance of hierarchical porous carbon microspheres prepared by simple one-pot method

Qinglan Zhao, Xianyou Wang*, Chun Wu, Jing Liu, Hao Wang, Jiao Gao, Youwei Zhang, Hongbo Shu*

Key Laboratory of Environmentally Friendly Chemistry and Applications of Ministry of Education, School of Chemistry, Xiangtan University, Xiangtan 411105, China

HIGHLIGHTS

- Hierarchical porous carbon microspheres are synthesized under mild condition by one-pot method.
- Pore structures of HPCMSs can be tailored by adjusting the reactant parameters.
- HPCMSs possess a pore combination of micro-, meso- and macropores with part graphitic layers.
- The energy density of HPCMS supercapacitor is still as high as 6.1 Wh kg^{-1} even at 5000 W kg^{-1}.

ARTICLE INFO

Article history:
Received 3 August 2013
Received in revised form
16 December 2013
Accepted 19 December 2013
Available online 31 December 2013

Keywords:
Supercapacitor
Hierarchical porous carbon microsphere
Simple one-pot method
Furfuryl alcohol

ABSTRACT

The hierarchical porous carbon microspheres (HPCMSs) using furfuryl alcohol as carbon resource have been prepared by a simple one-pot method. The HPCMSs are characterized by scanning electron microscopy (SEM), transmission electron microscopy (TEM) and nitrogen adsorption/desorption isotherm at 77 K, cyclic voltammetry (CV), galvanostatic charge/discharge tests, electrochemical impedance spectroscopy (EIS) and cycle life measurements in 6 M KOH. The results show that all the HPCMSs samples, which can be fabricated by adjusting the ratio of furfuryl alcohol/tetraethyl orthosilicate, possess three-dimensionally tailored pore structures with unique micro-, meso- and macroporous systems. Particularly, the HPCMS-2 prepared at the mole ratio of 2/1 (furfuryl alcohol/tetraethyl orthosilicate) shows the largest specific surface area of 709 m^2 g^{-1}, and the HPCMS-2 electrode owns specific capacitance as high as 221 F g^{-1} at the current density of 1 A g^{-1}. The supercapacitor using HPCMS-2 as the active material shows high specific capacitance and excellent cycle stability, which exhibits a specific capacitance of 56 F g^{-1} at the charge/discharge current density of 0.5 A g^{-1}. Furthermore, the HPCMS-2 supercapacitor delivers high energy densities of 6.1 Wh kg^{-1} at the power density of 5000 W kg^{-1}, revealing a promising application in supercapacitors.

1. Introduction

Supercapacitors as novel devices for storing energy, which are divided into electrical double layer capacitors (EDLCs) and pseudocapacitors, have attracted more and more attention for their long cycle life, good reversibility, high power density, etc [1,2]. The activated porous carbon materials as the most widely used supercapacitor materials have the advantages of high conductivity, electrochemical stability, open porosity and low cost [3]. Whereas, the slow ion transportation in small micropores of activated porous carbon materials restricts their effective utilization http://www.sciencedirect.com/science/article/pii/S0378775312006738 [4]. Moreover, the porosity of carbon materials plays an important role in the electrochemical capacitive performance of supercapacitors, especially for EDLCs [5]. It is well known that macropores serving as ion-buffering reservoirs are able to minimize the diffusion distances, mesopores can decrease ion-transport resistance, and micropores are capable of increasing the electric-double-layer capacitance [6–10]. As a consequence, hierarchical porous carbons with a pore combination of micro-, meso- and macropores hold great potential for high performance supercapacitor applications [11–13].

Recently, many efforts have been made to prepare hierarchical porous carbons. Xia et al. obtained hierarchical porous carbons of higher capacitance by CO_2 activation, which achieved the

* Corresponding authors. Tel.: +86 731 58292060; fax: +86 731 58292061.
E-mail addresses: wxianyou@yahoo.com (X. Wang), shu.hongbo@163.com (H. Shu).

0378-7753/$ – see front matter © 2013 Elsevier B.V. All rights reserved.
http://dx.doi.org/10.1016/j.jpowsour.2013.12.091

maximum specific capacitance of 206 F g^{-1} at the scan rate of 5 mV s^{-1} in 6 M KOH [14]. Bhattacharjya et al. synthesized hierarchical hollow core mesoporous shell carbon capsules via a nanocasting technique using the submicrometer sized solid core/mesoporous shell silica microspheres as templates, which exhibited a capacitance of 162 F g^{-1} at 0.3 A g^{-1} in two electrode symmetric system in organic electrolyte [15]. Liu et al. prepared hierarchical porous carbons by CO_2 and KOH activation processes, which delivered a capacitance of 250 F g^{-1} at 0.5 A g^{-1} in 6 M KOH [16]. Ma et al. synthesized Micro- and mesoporous carbon spheres (MMCSs) by templating method and further potassium hydroxide (KOH) activation, which showed a specific capacitance of 314 F g^{-1} at 0.5 A g^{-1} in 6 M KOH [17]. Our group fabricated activated hierarchically porous carbons (HPCs) using nickel oxide and surfactant as the dual template with further activation by HNO_3 [18]. Later, the effects of surfactant template concentration on the supercapacitive behaviors of the activated HPCs were investigated, and the activated HPCs-3 which was prepared at $C_{CTAB} = 0.27$ mol L^{-1} displayed the maximum specific capacitance of 272 F g^{-1} at the scan rate of 1 mV s^{-1} [19]. However, the above reported methods to obtain hierarchical porous carbons were time-consuming, energy-intensive, or complex due to the extra synthesis of special templates, additional activation and multi-step process. As a result, hierarchical porous carbons with high supercapacitive performance prepared through a simple time-saving and energy-conservative means are urgent to be explored.

To the best of our knowledge, there are few reports about methods of one-pot procedure on preparing hierarchical porous carbon microspheres. Herein, hierarchical porous carbon microspheres are synthesized under mild condition by one-pot method which is different from the previous complex and multi-step routes. Moreover, the physical and electrochemical properties of the as-prepared hierarchical porous carbon microspheres with three-dimensionally tailored pore structures by adjusting the reactant content are studied in detail.

2. Experimental

2.1. HPCMSs synthesis

The preparation strategy is shown in Fig. 1. HPCMSs were prepared by self-assembly of cetyltrimethyl ammonium bromide (CTAB), polyacrylic acid (PAA), tetraethyl orthosilicate (TEOS) and furfuryl alcohol (FA). Firstly, the anionic polyelectrolyte PAA and cationic surfactant CTAB micelles co-organized into complex particles by the electrostatic attraction between them. After the addition of TEOS and FA, they penetrated in the interspaces between the complex particles formed by PAA and CTAB micelles, and then TEOS hydrolyzed in situ in alkaline environment. Meanwhile the hydrolyzed negatively charged silica oligomers disturbed the electrostatic attraction between PAA and CTAB, and the co-assembly of the mesomorphous PAA/CTAB complexes was also perturbed. Next, the silica oligomers cross-linked around cationic surfactant CTAB micelles with the FA filling the interspaces, and PAA chains separated from the PAA/CTAB complexes to form PAA chain domains. After the calcination of the mixture, the carbon/SiO_2 composites were formed. Finally, when the silica was dissolved in 46% HF solution, the HPCMSs were obtained with a combination of micropores (templated by the TEOS-generated silica), mesopores (templated by CTAB micelles), and macropores (templated by phase-separated PAA). In a typical procedure, 0.55 g of CTAB was dissolved in 25.0 mL of deionized water, and 6.0 g of PAA (25 wt% solution) was added under continuous stirring to obtain a clear solution. The solution was supplied with 2.2 mL of ammonia (25%–28%) and became a milky mixture. After additional 20 min of stirring, 2.08 g of TEOS and various amounts of FA were added to the above mixture at a mole ratio of FA/TEOS in the range of 1.0–3.0. After further stirring for 15 min, the mixture was transferred into an autoclave, and then kept at 80 °C for 48 h. Subsequently, the mixture was evaporated at 50 °C to obtain FA/silica gel film. The FA/silica composite was polymerized at 150 °C for 6 h, and calcined at 900 °C for 3 h under an Ar flow to prepare carbon/SiO_2 composite. The heating rate was 2 °C min^{-1} below 600 °C and 5 °C min^{-1} above 600 °C. The as-prepared carbon/SiO_2 composite was immersed in an excess amount of 46% aqueous HF solution to dissolve silica, followed by washing with deionized water and drying to obtain hierarchically porous carbon microspheres. The synthesized hierarchically porous carbon microspheres were named as HPCMS-*x*. "HPCMS-*x*" denotes hierarchically porous carbon microsphere samples, wherein *x* represents the mole ratio of FA/TEOS.

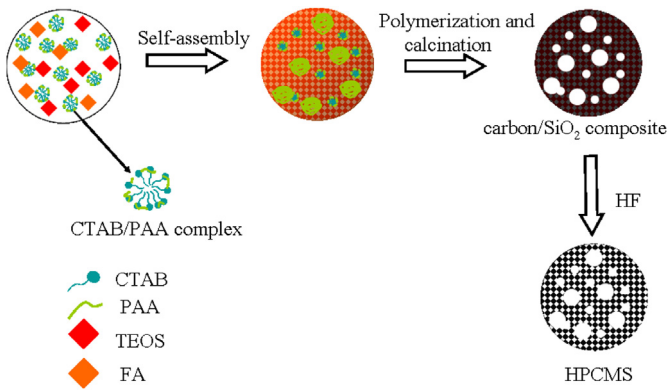

Fig. 1. Schematic illustration of preparation strategy of HPCMSs.

2.2. Characterization

The morphology and microstructure of the synthesized HPCMSs were characterized by scanning electron microscopy (SEM, JSM-6610LV, JEOL) and transmission electron microscopy (TEM, JEM-2100F, JEOL). The microstructure of HPCMSs was evaluated by X-ray diffractometer (XRD, D/MAX-3C, Rigaku) using Cu Kα radiation (30 kV, 30 mA, $\lambda = 1.5418$ Å). The specific surface area and pore structure of the HPCMSs were determined by N_2 adsorption/desorption isotherm at 77 K (JW-BK112) after the prepared samples were degassed at 110 °C overnight. The specific surface areas were calculated by the conventional Brunauer–Emmett–Teller (BET) method. Micropore volumes (V_{mic}) of the samples were analyzed by Horvath–Kawazoe (HK) theory. Pore volumes (V_{total}) and the pore size distribution (PSD) plot were derived from the adsorption branch of the isotherm based on the Barrett–Joyner–Halenda (BJH) model.

2.3. Electrochemical measurements

To prepare the EDLC electrode, 80 wt% the HPCMS sample, 10 wt % acetylene black and 10 wt% polyvinylidene fluoride (PVDF) binder were well mixed to get a slurry by adding *N*-methyl-2-pyrrolidone as a solvent. The slurry was filled into the nickel foam substrate using a spatula, dried at 80 °C overnight, and then pressed at 16 MPa for 1 min in order to assure a good electronic contact between the nickel foam substrate and the active material. Finally, the as-prepared electrode was dried at 80 °C in vacuum for 24 h.

The electrochemical performances of the as-prepared electrode were characterized by cyclic voltammetry (CV), galvanostatic charge/discharge tests and electrochemical impedance spectroscopy (EIS) on

an electrochemical workstation, (VersaSTAT3, Princeton Applied Research, USA). The CV measurements were performed between −1.0 V and 0 V at different scan rates varying from 5 mV s^{-1}–50 mV s^{-1}. Galvanostatic charge/discharge measurements were conducted from −1.0 V and 0 V at different constant current densities from 1 A g^{-1}–5 A g^{-1}. EIS measurements were recorded in the frequency range from 10^5 Hz to 10^{-2} Hz at a constant direct current bias potential of 0.2 V with amplitude of 5 mV. The experiments of CV, galvanostatic charge/discharge measurements and EIS were carried out using a three-electrode system, in which the prepared electrode (radius = 0.5 cm), a nickel sheet (10 cm × 8 cm) and a Hg/HgO electrode were used as the working, counter and reference electrodes, respectively. The cycle life was measured by a supercapacitor test station (SCTS, Arbin Instruments, USA) on button cell supercapacitors assembled according to the order of electrode-separator-electrode. All tests were measured in 6 M KOH electrolyte at room temperature.

3. Results and discussion

3.1. Structure analysis

In order to characterize the morphology and microstructure of the prepared HPCMSs, the representative SEM and TEM images are shown in Fig. 2. It can be seen from Fig. 2a–c that all the samples are three-dimensionally microsphere-like carbons with a considerable rough surface, suggesting abundantly open and accessible pores. As shown in Fig. 2a, there are some partial defects and fragments in HPCMS-1 resulting from etch of large amount silica. On the contrary, there is large carbon domain in HPCMS-3 due to the excess FA, as presented in Fig. 2c. HPCMS-2 is well-defined 3D microspheres with rough surface, as displayed in Fig. 2b. The TEM image (Fig. 2d) of HPCMS-2 further demonstrates the microsphere-like morphology and the hierarchical pore structure. High-resolution TEM measurements (Fig. 2e and f) are also conducted

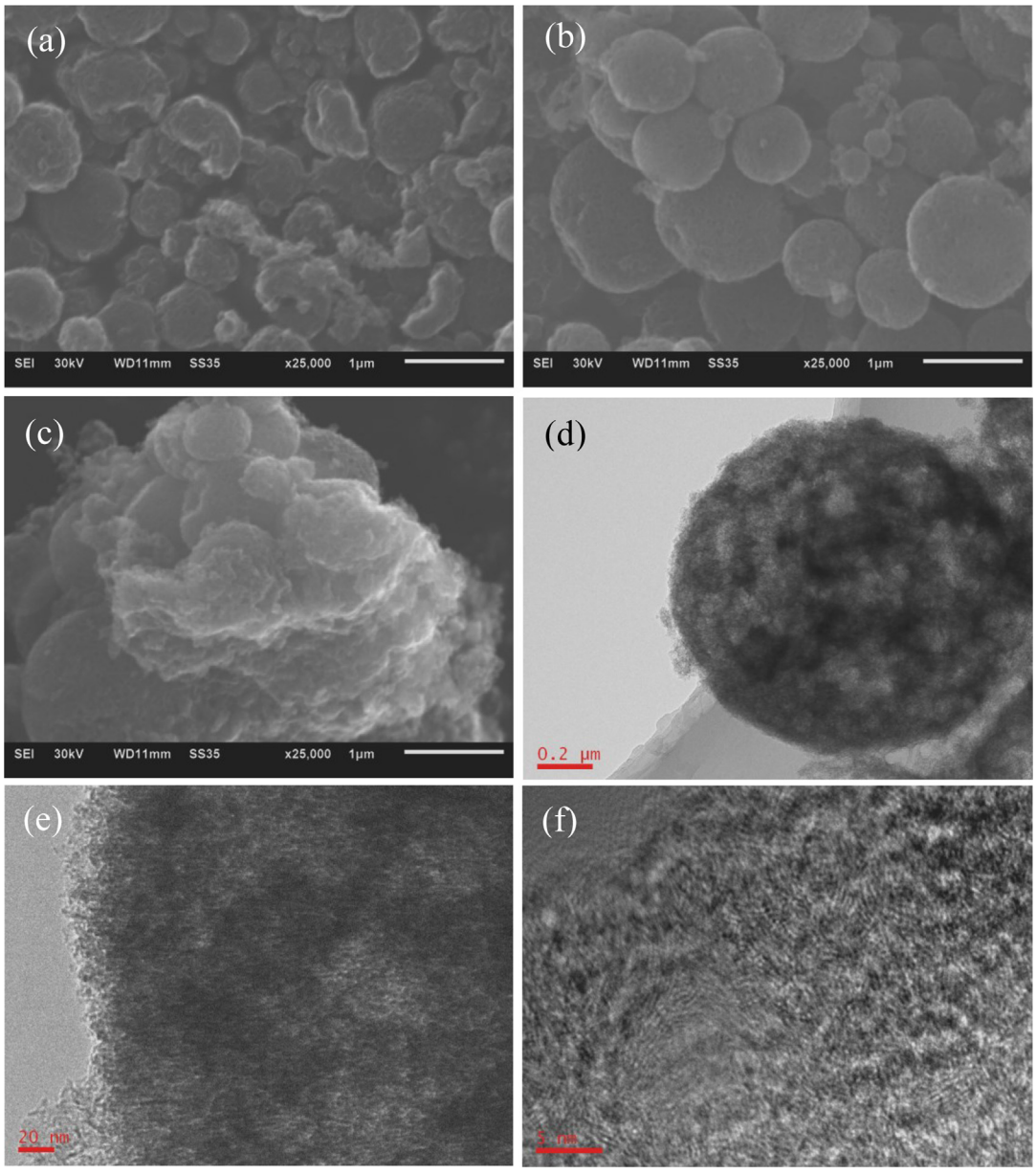

Fig. 2. SEM images of (a) HPCMS-1, (b) HPCMS-2 and (c) HPCMS-3; TEM image (d) and HRTEM images (e and f) of HPCMS-2.

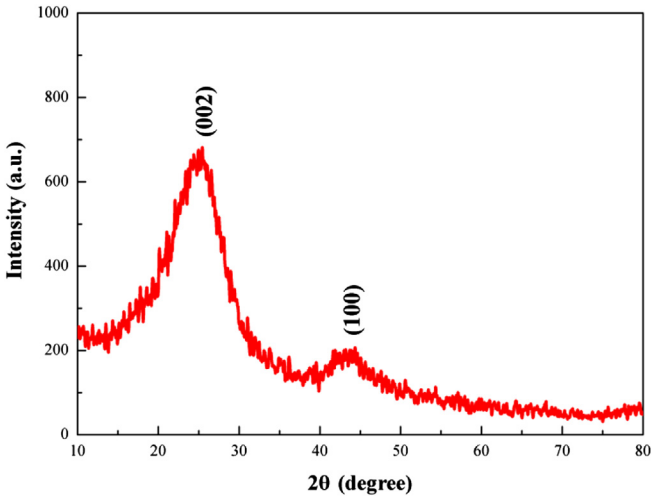

Fig. 3. XRD pattern of HPCMS-2.

to investigate the porous textures of HPCMS-2. As shown in Fig. 2e, it can be manifested that HPCMS-2 has a well-developed 3D-interconnected hierarchical pore system containing micropores, mesopores and macropores, where the bright part corresponds to the pores in carbon microspheres. The macropores can act as an electrolyte solution buffering reservoir; meanwhile, the mesopores and micropores devoting to diffusion and adsorption of electrolyte ions, are beneficial to mass transportation [20]. This kind of hierarchical porous structure can remarkably facilitate the fast penetration of the electrolyte into the pores, which could produce good electrochemical performance. What's more, there exist some graphitic layers, as shown in Fig. 2f, which could enhance electric conductivity of electrode materials [21,22]. These properties will be demonstrated by following measurements.

To further confirm the existence of graphitic layers, the XRD pattern of a typical sample of HPCMSs is shown in Fig. 3. It can be found that HPCMS-2 displays two broad diffraction peaks at around $2\theta = 25^\circ$ and 44°, which are corresponding to the (002) and (100) reflection of graphite, respectively. Apparently, the result of XRD is in good agreement with one of TEM images (Fig. 2f), and indicating the existence of the part graphitic layers.

The specific textural properties of the synthesized HPCMSs were further verified by the N_2 adsorption/desorption isotherm and BJH pore size distribution, and the results are shown in Fig. 4. All the nitrogen adsorption/desorption isotherms of the HPCMSs are a

Table 1
Textural properties and the fitting data for impedance spectra of HPCMSs.

Samples	FA/TEOS ratio	S_{BET} ($m^2\ g^{-1}$)	Average pore size (nm)	V_{total} ($m^3\ g^{-1}$)	V_{mic} ($m^3\ g^{-1}$)	R_I (Ω)	R_{CT} (Ω)	C_{dl} ($F\ g^{-1}$)	C_p ($F\ g^{-1}$)
HPCMS-1	1	509	7.92	1.01	0.20	1.55	0.13	91	29
HPCMS-2	2	709	4.61	0.88	0.27	1.39	0.15	114	30
HPCMS-3	3	476	7.19	0.88	0.18	1.58	0.2	83	32

combination of type II and type IV (according to IUPAC classification), as shown in Fig. 4a, suggesting the existence of both meso- and macroporosity [23–25]. The sharp increases at low pressure region ($P/P_0 < 0.05$) demonstrate the presence of micropores originating from the dissolution of the TEOS-generated silica [26,27]. The hysteresis loops at medium relative pressure can be interpreted as the capillary condensation in the mesopores probably deriving from removal of CTAB micelles or CTAB/PAA complexes [28]. Hysteresis loop tails at high relative pressure region ($P/P_0 > 0.95$) indicate the existence of macropores which may be generated from secondary nanopores formed by phase-separated PAA or interstice between HPCMSs particles [29].

The BJH pore size distributions of HPCMSs, which match well with the N_2 adsorption–desorption isotherms and the results of the TEM data, are shown in Fig. 4b. It is seen that all of the HPCMSs have a broad pore size distribution ranging from micropores to macropores, especially, HPCMS-2 owns the highest content of mesopores in which the pore size concentrates at 2–5 nm. Furthermore, the pore structures of HPCMSs could be affected by the ratio of FA and TEOS. When too low amount of FA is added (the ratio of FA/TEOS is 1), the mesostructure of HPCMSs will collapse during the silica removal due to the low carbon content, and as a result the quantity of macropores would increase. Nevertheless, when too much FA is added (the ratio of FA and TEOS is 3), excess FA will form a FA domain covering some pores, which can be also seen in Fig. 2c. The textural properties of all HPCMSs are listed in Table 1. The BET specific surface area are 509, 709, 476 $m^2\ g^{-1}$ for HPCMS-1, HPCMS-2 and HPCMS-3, respectively. Likewise, the micropore volumes for the above HPCMSs are 0.20, 0.27, 0.18 $cm^3\ g^{-1}$ by Horvath–Kawazoe (HK) theory, respectively. It can be found that HPCMS-2 acquires the largest specific surface areas and microporous volume. The hierarchical pore structures of the samples can facilitate the diffusion of ions and improve charge accumulation. It can be predicted that the HPCMSs will have a perspective application in supercapacitors and the HPCMS-2 will exhibit the best supercapacitive behaviors among all prepared HPCMSs samples.

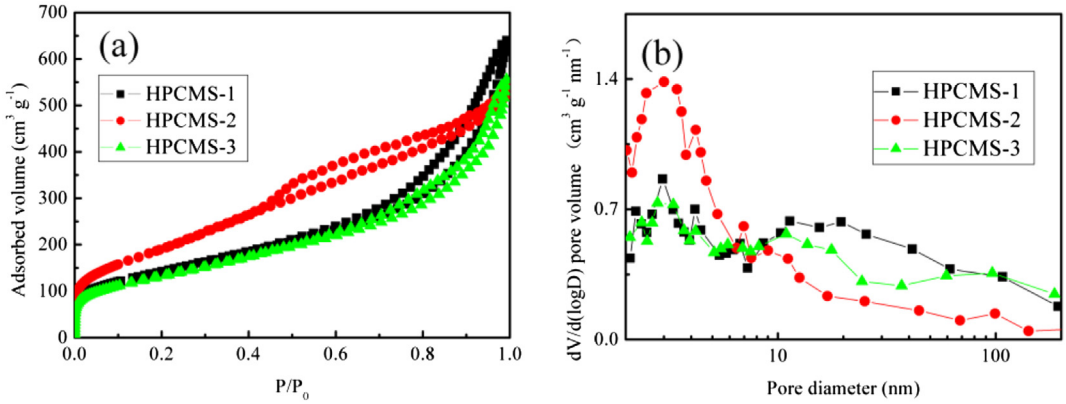

Fig. 4. (a) Nitrogen adsorption/desorption isotherms at 77 K of HPCMSs and (b) their corresponding BJH mesopore size distribution curves.

3.2. Electrochemical characterization

Cyclic voltammetry measurement was conducted to evaluate the electrochemical performance of the HPCMSs. Fig. 5a shows the cyclic voltammograms of HPCMSs electrodes at a scan rate of 5 mV s^{-1} between −1.0 V and 0 V vs. Hg/HgO in 6 M KOH. It can be observed that all the CV curves show a nearly rectangular shape, indicating nearly ideal capacitive behavior and excellent reversibility [30]. Usually, the capacitance of the carbon materials can be estimated by Eq. (1):

$$C_s = \frac{I_a + |I_c|}{2m(dV/dt)} \quad (1)$$

where C_s, I_a, I_c, m and dV/dt are the specific capacitance (F g^{-1}), the current (A) of anodic and cathodic CV curves on positive and negative sweeps, the mass of active material (g), and the sweep rate (mV s^{-1}), respectively [31]. The specific capacitances (C_s) are 149 F g^{-1}, 171 F g^{-1} and 144 F g^{-1} at the scan rate of 5 mV s^{-1} determined by Eq. (1) for HPCMS-1, HPCMS-2 and HPCMS-3, respectively, owing to the different pore structures of HPCMSs which are prepared by adjusting the ratio of FA/TEOS. Fig. 5b further presents the relationship of specific capacitances and scan rates for HPCMSs electrodes. It can be observed that the specific capacitance of HPCMS-2 is the highest at the same scan rate. Moreover, the capacitance loss is only about 18% with the scan rate increasing from 5 mV s^{-1}–50 mV s^{-1}. Simultaneously, two capacitance lines of HPCMS-1 and HPCMS-3 are overlapped a little in the scan rate range of 20–50 mV s^{-1}, which may be attributed to their similar pore size distributions (Fig. 4b). The high current response of HPCMS-2 can be ascribed to the hierarchical pore structures facilitating fast mass transportation and decreasing ion-transport resistance.

Representative galvanostatic charge/discharge behaviors are often investigated to estimate electrochemical performance of electrode. Fig. 5c and d display the galvanostatic charge/discharge profiles of the HPCMSs electrodes. The charge/discharge curves of all HPCMSs are generally symmetric triangular shapes, illustrating that the HPCMSs have typical supercapacitive behaviors of porous carbon and excellent capacitive reversibility, which is in well agreement with CV observations. The specific capacitances of the HPCMSs electrodes can be calculated from Eq. (2):

$$C_m = \frac{I \times \Delta t}{\Delta V \times m} \quad (2)$$

where C_m, I, Δt, ΔV and m are the specific capacitance (F g^{-1}), the discharge current (A), the discharge time (s), the potential window (V) and the weight of active material (g), respectively [32]. It can be observed that the maximum specific capacitance is as high as 221 F g^{-1} for HPCMS-2 at the current density of 1 A g^{-1}. Furthermore, in Fig. 5c insert, all HPCMSs exhibit relatively small IR drop at the beginning of the initial discharging process. Particularly, the IR drop of HPCMS-2 is the least of all sample electrodes. The IR drop is an effective measurement of equivalent series resistance which influences the overall power performance of supercapacitors [33].

The charge/discharge curves of HPCMS-2 at different current densities are shown further in Fig. 5d. It can be noted from Fig. 5d that all the curves are commonly linear and symmetrical. The specific capacitance of HPCMS-2 electrode decreases with the current density increasing from 1 A g^{-1}–5 A g^{-1}. This can be ascribed to the diffusion limitation of electrolyte ions into small

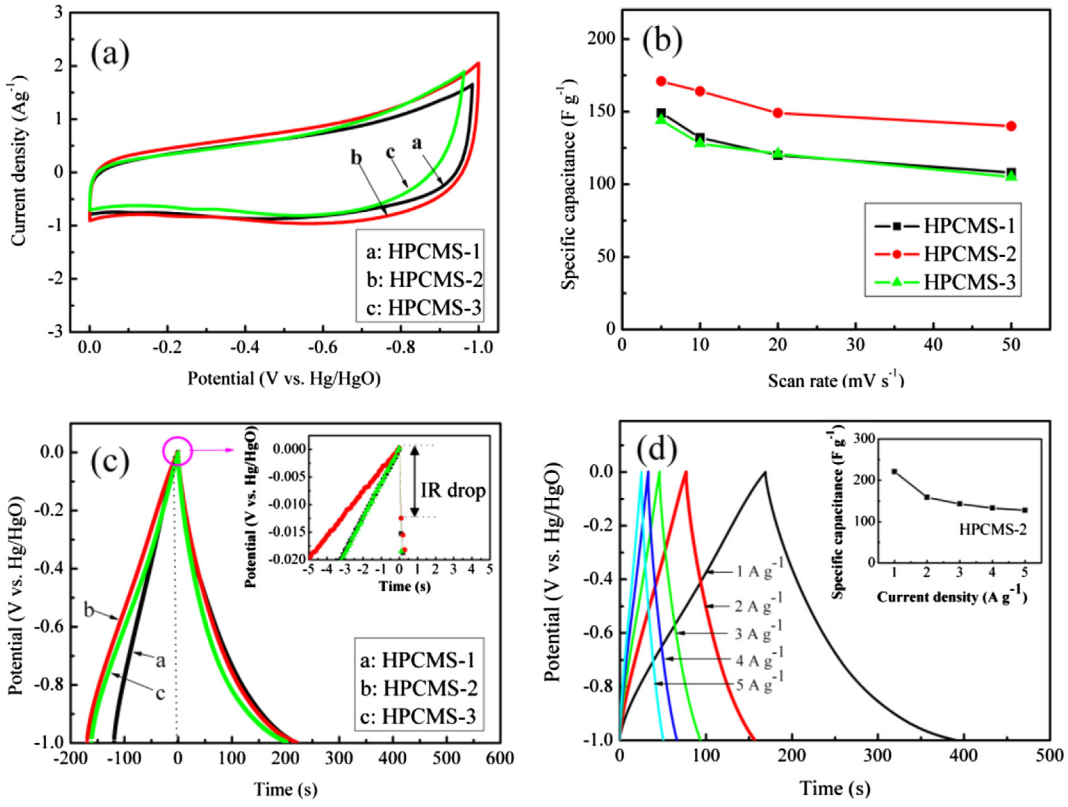

Fig. 5. (a) Cyclic voltammograms of HPCMSs electrodes at a scan rate of 5 mV s^{-1}; (b) Specific capacitances of HPCMSs at different scan rates; (c) Galvanostatic charge/discharge curves of HPCMSs electrodes at the current density of 1 A g^{-1} with the IR drop insert; (d) Charge/discharge curves for HPCMS-2 electrode at different current densities, and inset is its specific capacitance at different current densities.

pores under high current density [34]. Fig. 5d inset gives the specific capacitance of HPCMS-2 electrode as a function of current density. The retention of specific capacitance can maintain over 57% with the current density changing from 1 A g^{-1}–5 A g^{-1}, suggesting a good rate capability, which is associated with the fast ion transportation. Thus, the HPCMS-2 is a prospective electrode material for the application of supercapacitor.

Electrochemical impedance spectroscopy is a potent means to analyze capacitive behaviors of porous carbon material. Fig. 6a displays Nyquist plots of impedance spectra measured for HPCMSs electrodes which can be fitted by the equivalent circuit as shown in Fig. 6c. The impedance spectra are almost similar with an arc in the high-frequency region and a straight line in the low frequency region. The representative impedance response is typical capacitive behavior of porous carbon electrodes. The crossover point of the highest frequency with the real part of the impedance is internal resistance (R_I), which consists of the solution resistance, the intrinsic resistance of the electroactive material and the contact resistance between electroactive materials and current collector [35]. The semicircle loop diameter in the high-frequency region corresponds to the charge-transfer resistance (R_{CT}) across the electrode/solution interface [36]. The straight line in the low-frequency region leans more toward the imaginary axis, revealing good capacitive behavior [37]. The double-layer capacitance (C_{dl}) and the pseudocapacitance (C_p) fitted for impedance spectra of HPCMSs electrodes based on ZSimpWin software are listed in Table 1. It is worth noting that the HPCMS-2 electrode exhibits low internal resistance and charge-transfer resistance of 1.39 Ω and 0.15 Ω, respectively.

The curves of the specific capacitance with the frequency for the different HPCMSs electrodes are shown in Fig. 6b. The specific capacitance is determined by the Eq. (3):

$$C = -\frac{1}{2\pi f Z'' m} \tag{3}$$

where C, f, Z'' and m are the specific capacitance (F g^{-1}), the frequency (Hz), the imaginary impedance (Ω) and the mass of active material (g), respectively [38]. The HPCMS-2 electrode achieves the

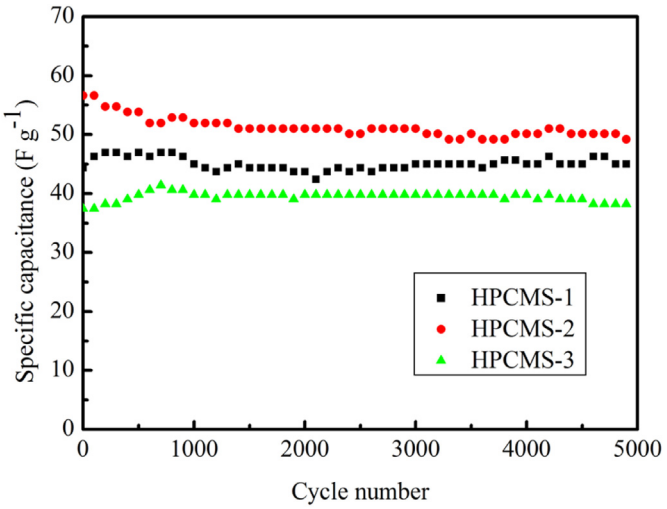

Fig. 7. Cyclic performance for HPCMSs supercapacitors at a current density of 0.5 A g^{-1}.

specific capacitance of 135 F g^{-1} at low frequency range approximately to 0.01 Hz, which is higher than those of HPCMS-1 (119 F g^{-1}) and HPCMS-3 (115 F g^{-1}) electrodes due to its optimal hierarchical porous structure. Moreover, the trend of the specific capacitances for HPCMSs electrodes evaluated from the low-frequency data of the spectra is consistent with the results of CV and charge–discharge tests.

Long cycle life is one of the most crucial parameters for the supercapacitor application [39]. As shown in Fig. 7, the cycle life curves of HPCMSs supercapacitors were measured in 6 M KOH at a current density of 0.5 A g^{-1}. The initial capacitances are as high as 47 F g^{-1}, 56 F g^{-1} and 41 F g^{-1} for HPCMS-1, HPCMS-2, and HPCMS-3 supercapacitors, respectively. Besides, the specific capacitance of HPCMS-2 supercapacitor after 5000 cycles is higher than the other samples. It can be attributed to its stable hierarchical porous structure and high specific surface area.

The galvanostatic charge/discharge curves of different HPCMSs supercapacitors tested under current densities ranging from

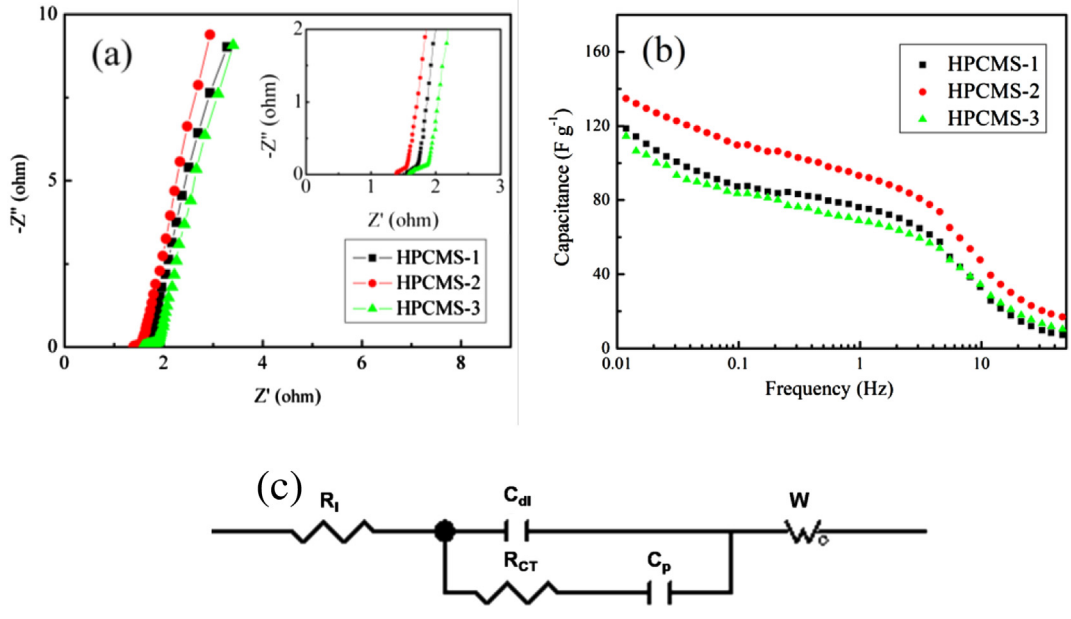

Fig. 6. (a) The Nyquist plots of different HPCMSs electrodes with the expanded high-frequency region of the plot inset; (b) The curves of the specific capacitance with the frequency for the different HPCMSs electrodes; (c) Equivalent circuit for the impedance spectra of HPCMSs electrodes.

1 A g^{-1}–10 A g^{-1} are shown in Fig. 8a–c. It can be found that all the galvanostatic charge/discharge curves of HPCMSs supercapacitors are generally symmetric, indicating typical capacitive behavior. The specific capacitances of HPCMS-1, HPCMS-2 and HPCMS-3 supercapacitors at 10 A g^{-1} are 34 F g^{-1}, 44 F g^{-1} and 29 F g^{-1}, respectively. Additionally, the HPCMS-2 supercapacitor delivers specific capacitances of 49 F g^{-1}, 46 F g^{-1}, 45 F g^{-1} and 44 F g^{-1} at 1 A g^{-1}, 2 A g^{-1}, 5 A g^{-1} and 10 A g^{-1}, respectively. The loss of capacitance is only 10% when the current density increases from 1 A g^{-1}–10 A g^{-1}, which reveals good capacitive property resulting from its high specific surface area and hierarchical porous structure.

Power density and energy density as important parameters are used to evaluate the capacitive performance of electrochemical cells. As shown in Fig. 8d, the Ragone plots display the relationship between power density and energy density. The energy and power densities are calculated by means of galvanostatic charging–discharging of supercapacitor at current densities ranging from 1 A g^{-1}–10 A g^{-1}, according to Eqs. (4) and (5), respectively [40]:

$$E = \frac{1}{2}CV^2 \tag{4}$$

where E, C and V are the energy density (Wh kg^{-1}), the specific capacitance of the two-electrode capacitor (F g^{-1}) and the cell voltage (V), respectively.

$$P = \frac{E}{\Delta t} \tag{5}$$

where P, E and Δt are the power density (W kg^{-1}), the energy density (Wh kg^{-1}) and discharge time (s), respectively. All the Ragone plots show similar trends in which the energy density drops with the power density increasing. The energy and power limitations observed at high rates are related to the resistance and the diffusion pathways within the porous textures [41]. It can be found in Fig. 8d that the energy density of HPCMS-2 supercapacitor at the same power density is the highest among all three samples, which means that the HPCMS-2 supercapacitor is superior to HPCMS-1 and HPCMS-3 supercapacitors in terms of both energy and power. The high energy density of 6.8 Wh kg^{-1} is achieved for HPCMS-2 supercapacitor at the power density of 500 W kg^{-1}, and still remains 6.1 Wh kg^{-1} even at the power density of 5000 W kg^{-1}. The results demonstrate that the HPCMS-2 supercapacitor possesses great potential for high energy and power density electrochemical supercapacitor.

4. Conclusions

In summary, hierarchical porous carbon microspheres have been successfully obtained via a one-pot procedure distinct from multi-step procedures in the conventional templating methods. It's worthy of being noted that the pore structures can be controlled by adjusting the ratio of FA/TEOS from 1/1 to 3/1. All the fabricated hierarchical porous carbon samples are 3D-interconnected carbon microspheres possessing large specific surface areas and wide pore-size distributions from micropores to macropores. Particularly, the HPCMS-2 sample prepared at the mole ratio of 2/1 (FA/TEOS) presents the largest BET specific surface area of 709 m^2 g^{-1} and the average pore size of 4.61 nm, with part graphitic layers. Additionally, all of the synthesized HPCMSs show high current response, excellent capacitive reversibility, small ohmic resistance and long cycle life. Coinciding with the results of structure analysis, the HPCMS-2 achieves the maximum capacitance of 171 F g^{-1} at the scan rate of 5 mV s^{-1} in 6 M KOH. Meanwhile, the HPCMS-2 owns a good rate performance and the high specific capacitance of 221 F g^{-1} at current density of 1 A g^{-1}, as well as low internal

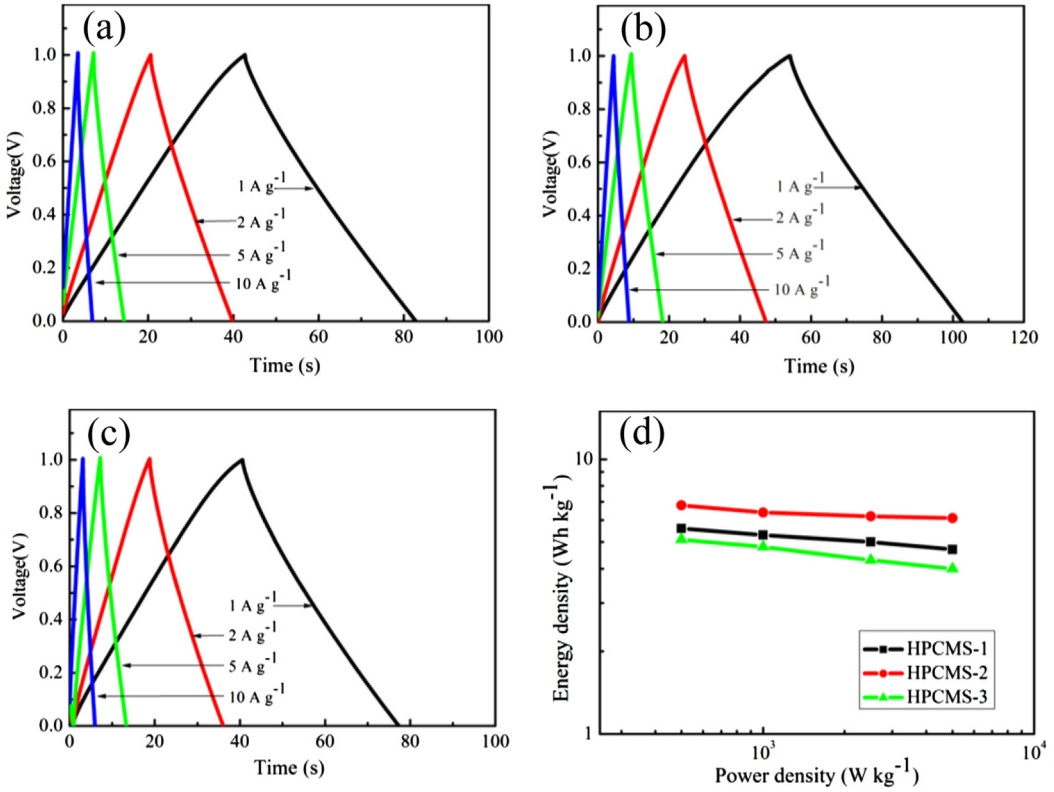

Fig. 8. Galvanostatic charge/discharge curves of HPCMS-1 (a), HPCMS-2 (b) and HPCMS-3 (c) supercapacitors at current densities ranging from 1 A g^{-1}–10 A g^{-1}; Ragone plots of HPCMSs supercapacitors measured at current densities varying from 1 A g^{-1}–10 A g^{-1} (d).

resistance and charge-transfer resistance of 1.39 Ω and 1.54 Ω. Furthermore, the supercapacitor based on HPCMS-2 electrodes exhibits excellent stability, of which the specific capacitance is as high as 56 F g^{-1}. Additionally, the HPCMS-2 supercapacitor shows the high energy density of 6.8 Wh kg^{-1} at the power density of 500 W kg^{-1}, and still is as high as 6.1 Wh kg^{-1} even at the power density of 5000 W kg^{-1}. The remarkable supercapacitive performance may be ascribed to its hierarchical pore structure and high surface area. Therefore, the HPCMS-2 is a promising candidate in application of high performance supercapacitors.

Acknowledgments

This work was financially supported by the National Natural Science Foundation of China (Grant Nos. 51072173, 51272221, 51302239 and 21203161), the Natural Science Foundation of Hunan Province, China (Grant No. 13JJ4051), the Scientific Research Fund of Hunan Provincial Education Department (Grant No. 12C0395).

References

[1] M.F. Shao, F.Y. Ning, Y.F. Zhao, J.W. Zhao, M. Wei, D.G. Evans, X. Duan, Chem. Mater. 24 (2012) 1192–1197.
[2] H. Kim, M.E. Fortunato, H.X. Xu, J.H. Bang, K.S. Suslick, J. Phys. Chem. C 115 (2011) 20481–20486.
[3] P. Simon, Y. Gogotsi, Nat. Mater. 7 (2008) 845–854.
[4] Y. Han, X.T. Dong, C. Zhang, S.X. Liu, J. Power Sources 211 (2012) 92–96.
[5] G. Lota, K. Fic, E. Frackowiak, Energy Environ. Sci. 4 (2011) 1592–1605.
[6] W.X. Chen, H. Zhang, Y.Q. Huang, W.K. Wang, J. Mater. Chem. 20 (2010) 4773–4775.
[7] A. Ghosh, Y.H. Lee, ChemSusChem 5 (2012) 480–499.
[8] Y.K. Lv, L.H. Gan, M.X. Liu, W. Xiong, Z.J. Xu, D.Z. Zhu, D.S. Wright, J. Power Sources 209 (2012) 152–157.
[9] Y. Li, Z.-Y. Fu, B.-L. Su, Adv. Funct. Mater. 22 (2012) 4634–4667.
[10] Y.Y. Li, Z.S. Li, P.K. Shen, Adv. Mater. 25 (2013) 2474–2480.
[11] H.-J. Liu, X.-M. Wang, W.-J. Cui, Y.-Q. Dou, D.-Y. Zhao, Y.-Y. Xia, J. Mater. Chem. 20 (2010) 4223–4230.
[12] F. Xu, R.J. Cai, Q.C. Zeng, C. Zou, D.C. Wu, F. Li, X.E. Lu, Y.R. Liang, R.W. Fu, J. Mater. Chem. 21 (2011) 1970–1976.
[13] J. Hu, H.L. Wang, X. Huang, Electrochim. Acta 74 (2012) 98–104.
[14] K.S. Xia, Q.M. Gao, J.H. Jiang, J. Hu, Carbon 46 (2008) 1718–1726.
[15] D. Bhattacharjya, M.-S. Kim, T.-S. Bae, J.-S. Yu, J. Power Sources 244 (2013) 799–805.
[16] D. Liu, J. Shen, N.P. Liu, H.Y. Yang, A. Du, Electrochim. Acta 89 (2013) 571–576.
[17] X.M. Ma, M.X. Liu, L.H. Gan, Y.H. Zhao, L.W. Chen, J. Solid State Electrochem. 17 (2013) 2293–2301.
[18] X.Y. Zhang, X.Y. Wang, Y.S. Bai, X.Y. Wang, J.C. Su, J. Electrochem. Soc. 159 (2012) A431–A437.
[19] X.Y. Zhang, X.Y. Wang, J.C. Su, X.Y. Wang, L.L. Jiang, H. Wu, C. Wu, J. Power Sources 199 (2012) 402–408.
[20] B.Z. Fang, J.H. Kim, M.S. Kim, J.S. Yu, Acc. Chem. Res. 46 (2013) 1397–1406.
[21] S.B. Yang, X.L. Feng, K. Müllen, Adv. Mater. 23 (2011) 3575–3579.
[22] L.L. Zhang, X.S. Zhao, Chem. Soc. Rev. 38 (2009) 2520–2531.
[23] D.J. Babu, M. Lange, G. Cherkashinin, A. Issanin, R. Staudt, J.J. Schneider, Carbon 61 (2013) 616–623.
[24] A. Bhunia, V. Vasylyeva, C. Janiak, Chem. Commun. 49 (2013) 3961–3963.
[25] B.Y. Liu, H.P. Huang, F.H. Zhang, Y. Zhou, W.G. Li, J.W. Zhang, Mater. Lett. 66 (2012) 199–202.
[26] Z.J. Zhang, C. Chen, P. Cui, X.Y. Chen, J. Power Sources 242 (2013) 41–49.
[27] J. Górka, M. Jaroniec, Carbon 49 (2011) 154–160.
[28] K. Cho, K. Na, J. Kim, O. Terasaki, R. Ryoo, Chem. Mater. 24 (2012) 2733–2738.
[29] W. Xia, B. Qiu, D.G. Xia, R.Q. Zou, Sci. Rep. (2013), http://dx.doi.org/10.1038/srep01935.
[30] Z. Chen, Y.C. Qin, D. Weng, Q.F. Xiao, Y.T. Peng, X.L. Wang, H.X. Li, F. Wei, Y.F. Lu, Adv. Funct. Mater. 19 (2009) 3420–3426.
[31] C. Wu, X.Y. Wang, B.W. Ju, L.L. Jiang, H. Wu, Q.L. Zhao, L.H. Yi, J. Power Sources 227 (2013) 1–7.
[32] S.J. Ding, T. Zhu, J.S. Chen, Z.Y. Wang, C.L. Yuan, X.W. (David) Lou, J. Mater. Chem. 21 (2011) 6602.
[33] S.R.S. Prabaharan, R. Vimala, Z. Zainal, J. Power Sources 161 (2006) 730–736.
[34] C. Zheng, W.Z. Qian, C.J. Cui, Q. Zhang, Y.G. Jin, M.Q. Zhao, P.H. Tan, F. Wei, Carbon 50 (2012) 5167–5175.
[35] T. Wua, J.Y. Li, L.R. Hou, C.Z. Yuan, L. Yang, X.G. Zhang, Electrochim. Acta 81 (2012) 172–178.
[36] P. Yu, X. Zhang, D.L. Wang, L. Wang, Y.W. Ma, Cryst. Growth Des. 9 (2009) 528–533.
[37] Z.B. Lei, Z.W. Chen, X.S. Zhao, J. Phys. Chem. C 114 (2010) 19867–19874.
[38] D. Kalpana, S.H. Cho, S.B. Lee, Y.S. Lee, Rohit Misra, N.G. Renganathan, J. Power Sources 190 (2009) 587–591.
[39] H.W. Wang, Y.L. Wang, Z.G. Hu, X.F. Wang, ACS Appl. Mater. Interfaces 4 (2012) 6827–6834.
[40] Z.J. Fan, J. Yan, T. Wei, L.J. Zhi, G.Q. Ning, T.Y. Li, F. Wei, Adv. Funct. Mater. 21 (2011) 2366–2375.
[41] D.W. Wang, F. Li, M. Liu, G.Q. Lu, H.M. Cheng, Angew. Chem. 120 (2008) 379–382.